On the Seasonal Cycles of Tropical Cyclone Potential Intensity

DANIEL M. GILFORD, SUSAN SOLOMON, AND KERRY A. EMANUEL

Department of Earth, Atmospheric and Planetary Sciences, Massachusetts Institute of Technology, Cambridge, Massachusetts

(Manuscript received 18 November 2016, in final form 21 April 2017)

ABSTRACT

Recent studies have investigated trends and interannual variability in the potential intensity (PI) of tropical cyclones (TCs), but relatively few have examined TC PI seasonality or its controlling factors. Potential intensity is a function of environmental conditions that influence thermodynamic atmosphere–ocean disequilibrium and the TC thermodynamic efficiency—primarily sea surface temperatures and the TC outflow temperatures—and therefore varies spatially across ocean basins with different ambient conditions. This study analyzes the seasonal cycles of TC PI in each main development region using reanalysis data from 1980 to 2013. TC outflow in the western North Pacific (WNP) region is found above the tropopause throughout the seasonal cycle. Consequently, WNP TC PI is strongly influenced by the seasonal cycle of lower-stratospheric temperatures, which act to damp its seasonal variability and thereby permit powerful TCs any time during the year. In contrast, the other main development regions (such as the North Atlantic) exhibit outflow levels in the troposphere through much of the year, except during their peak seasons. Mathematical decomposition of the TC PI metric shows that outflow temperatures damp WNP TC PI seasonality through thermodynamic efficiency by a quarter to a third, whereas disequilibrium between SSTs and the troposphere drives 72%–85% of the seasonal amplitude in the other ocean basins. Strong linkages between disequilibrium and TC PI seasonality in these basins result in thermodynamic support for powerful TCs only during their peak seasons. Decomposition also shows that the stratospheric influence on outflow temperatures in the WNP delays the peak month of TC PI by a month.

1. Introduction

It is important to understand the intensity of tropical cyclones (TCs) because coastal societies are vulnerable to their dangerous and costly impacts (e.g., Pielke and Pielke 1997). Studies over the last few decades have established a theoretical framework for investigating the potential intensity (PI) that a TC may reach given local environmental conditions (e.g., Emanuel 1985; Holland 1997; Bister and Emanuel 1998, 2002, hereafter BE02). Evidence suggests that variations in actual tropical cyclone intensities scale with variability in potential intensity on multiple time scales (Emanuel 2000; Wing et al. 2007). While it is recognized that warming sea surface temperatures (SSTs) have been and will continue to be a key driver for TC PI trends under anthropogenic climate forcing (e.g., Henderson-Sellers et al. 1998; Emanuel 2005; Knutson et al. 2010; Holland and Bruyère 2014; Strazzo et al. 2015; Walsh et al. 2016; and references therein), recent work has also focused on how lower-stratospheric temperatures influence TC PI (e.g., Emanuel et al. 2013; Ramsay 2013; Wang et al. 2014). Some studies have explored stratospheric linkages with TC PI trends over the past three decades (Emanuel et al. 2013; Wing et al. 2015), in the future under anthropogenic climate forcing (Vecchi et al. 2014; Sobel et al. 2016; Walsh et al. 2016), and in a Montreal Protocol world–avoided scenario (Polvani et al. 2016). Less attention has been given to interannual variability in TC PI and its connections with the middle atmosphere (Wing et al. 2015), and only a few studies have considered the seasonality of potential intensity (Free et al. 2004; Tonkin et al. 2000). In this study, we calculate the seasonal cycles of tropical cyclone potential intensity in the main TC development regions

Denotes content that is immediately available upon publication as open access.

Supplemental information related to this paper is available at the Journals Online website: http://dx.doi.org/10.1175/JCLI-D-16-0827.s1.

Corresponding author: Daniel M. Gilford, dgilford@mit.edu

DOI: 10.1175/JCLI-D-16-0827.1

with 34 years of reanalysis data and use a decomposition method to determine the main factors that drive TC PI seasonality in these regions.

Tonkin et al. (2000) investigated the seasonal cycles of TC potential intensity with a set of radiosonde stations in the northwestern Pacific, Australian southwestern Pacific, and North Atlantic regions. Potential intensity calculations using the early Emanuel (1985, 1991) method and the Holland (1997) method were compared to one another and to observed TC intensities. Tonkin et al. (2000) found that both methods generally performed well at predicting observed seasonal intensities in the tropics (though each was overly sensitive to certain environmental conditions). However, their study did not directly attribute the seasonal cycles to local thermodynamic contributions beyond SSTs, and their data were spatially limited. Free et al. (2004) also explored potential intensity seasonal cycles. Using data from 14 radiosonde stations, they showed that there were seasonal differences in TC PI across the tropics. In the Caribbean these differences were attributed to each station's distance from the equator (with calculations showing larger seasonal cycle amplitudes at stations farther from the equator), whereas no explanation was offered for the Pacific basin differences. Further, no analysis was performed to determine the thermodynamic conditions contributing to the seasonal cycles in each ocean basin. In this study, we will show that spatial differences in the seasonal cycles of TC PI are linked to the seasonality of each ocean basin's sea surface temperatures, TC outflow levels, and outflow temperatures. Note that we do not explore the seasonality of other factors known to be important for the genesis or intensity of tropical cyclones, such as vertical wind shear (e.g., Frank and Ritchie 2001; Emanuel 2006).

The goals of this study are to characterize the seasonal cycles of TC PI pertaining to the main TC development regions in each ocean basin and to identify the key factors contributing to these cycles. In section 2, we describe the TC PI calculation and decomposition, along with the reanalysis data used to compute TC PI. Section 3 shows the resulting TC PI seasonal cycles and quantifies the thermodynamic contributions to these cycles. The study is summarized in section 4.

2. Data and methods

Tropical cyclone potential intensity $V_{\max}$ is defined following Bister and Emanuel (1998):

$$V_{\max}^2 = \frac{C_k}{C_D}\frac{(T_s - T_o)}{T_o}(h_0^* - h^*), \tag{1}$$

where C_k and C_D are the enthalpy and momentum surface exchange coefficients, respectively; T_s is the sea surface temperature; T_o is the mean outflow temperature; h_0^* is the saturation moist static energy at the sea surface; and h^* is the moist static energy of the free troposphere. The ratio C_k/C_D is an uncertain quantity and determining its value is an area of active research (e.g., Emanuel 2003, and references therein), but it is typically taken to be a constant. Here we set $C_k/C_D = 0.9$ following the precedent of previous studies (Wang et al. 2014; Wing et al. 2015), but we have tested a range of reasonable ratios (0.4–1.0) and found our results to be qualitatively insensitive to the choice. The term $(T_s - T_o)/T_o$ is the thermodynamic efficiency of the potential tropical cyclone. It is readily determined that kelvin for kelvin the efficiency term is more sensitive to T_o than T_s. However, T_s seasonal amplitude is generally larger than T_o, and T_s and T_o may be related to one another through the outflow level, with key implications for the seasonal cycles of TC PI (see section 3). The final term $(h_0^* - h^*)$ is the thermodynamic disequilibrium between the sea surface and the free troposphere, which is principally controlled by sea surface temperatures (e.g., Emanuel 2007).

We compute the potential intensity using the algorithm of BE02. The BE02 scheme is more accurate for TC PI calculations in the tropics than directly calculating and summing each individual term on the right-hand side of Eq. (1) because of its incorporation of water loading and virtual temperature (Garner 2015; Wing et al. 2015). Besides its increased accuracy over direct computation of Eq. (1), the BE02 algorithm is advantageous because it has been frequently employed in previous studies of PI (e.g., Emanuel 2007; Sobel and Camargo 2011; Emanuel et al. 2013; Wang et al. 2014; Wing et al. 2015; Polvani et al. 2016), allowing straightforward comparisons between those studies and this work. We computed TC PI directly with Eq. (1) and found that the thermodynamic disequilibrium term is larger than that inferred from the BE02 algorithm by 10%–25%, but results are qualitatively similar to those in section 3.

The BE02 algorithm requires profiles of temperature and humidity, along with sea surface temperatures and mean sea level pressures. The algorithm is configured to output $V_{\max}$, the outflow temperature, and the outflow temperature level (OTL). The OTL is the level of neutral buoyancy for an air parcel saturated at sea level pressure, corresponding to the outflow temperature. Outflow temperatures allow direct calculation of the efficiency term [second term on the right-hand side of Eq. (1)] at each temporal and spatial location. Given the output potential intensity and efficiency, the thermodynamic disequilibrium $(h_0^* - h^*)$ can be derived from Eq. (1). In the BE02 algorithm, parcels are lifted

assuming reversible adiabatic ascent. Assuming pseudoadiabatic ascent instead leads to qualitatively similar results, except that OTLs are typically found at higher altitudes, allowing more stratospheric influence on TC PI in all regions (see section 3). We decompose Eq. (1) by taking the natural logarithm of both sides:

$$2\log(V_{\max}) = \log\left(\frac{C_k}{C_D}\right) + \log\left(\frac{T_s - T_o}{T_o}\right) + \log(h_0^* - h^*). \quad (2)$$

This log-additive model is advantageous because it quantifies thermodynamic disequilibrium and thermodynamic efficiency contributions to TC PI at every spatial and temporal location.

Temperature, water vapor, sea surface temperature, and mean sea level pressure data from 1980 to 2013 are taken from the second Modern-Era Retrospective Analysis for Research and Applications (MERRA-2; Bosilovich et al. 2016; NASA 2016) and the European Centre for Medium-Range Weather Forecasts interim reanalysis (ERA-Interim, hereafter ERA-I; Dee et al. 2011; ECMWF 2016). The 6-hourly data from both reanalyses are regridded onto a monthly 2.5° × 2.5° grid. As we average over tropical cyclone main development regions (see below), the horizontal resolution is not expected to play a significant role in the results. Previous work by Kossin (2015) validated observed TC cloud-top brightness temperatures against MERRA/ERA-I outflow temperatures and found that they vary consistently with one another on multiple time scales, suggesting that seasonal evaluation of TC outflow temperatures and potential intensity with these reanalyses is appropriate. For clarity and brevity we show only the MERRA-2 results herein; ERA-I results are largely consistent with MERRA-2 and are shown in the supplemental material (Figs. S1–S4).

Our methodology is designed to evaluate the seasonal cycles of potential intensity dictated by seasonal atmospheric and oceanic states. We determine the monthly means of each state variable from reanalyses and compute TC PI with the BE02 algorithm at every ocean grid point. Monthly means of state variables and algorithm outputs are then time averaged over the 34-yr period and area averaged over the tropical cyclone main development regions in each ocean basin (Table 1) following Emanuel (2005) and Wing et al. (2015), except that we retain the full seasonal cycle in each case (rather than averaging over the peak months) and use a somewhat different NA main development region definition than Wing et al. (2015). Our NA region focuses specifically on TC PI in the far-western Atlantic and Gulf of Mexico, where tropical cyclones frequently develop (e.g., Gray 1984); results for the NA are qualitatively insensitive to whether we use this definition or that of Wing et al. (2015). Furthermore, results for each main development region in Table 1 are qualitatively robust to modest (~5°) poleward shifts (see Fig. 2, described in greater detail below).

TABLE 1. TC main development regions and their geographical ranges. Regions (except NA; see text) are defined following Emanuel (2005) and Wing et al. (2015).

Basin	Range
North Atlantic (NA)	8.75°–31.25°N, 266.25°–308.75°E
Eastern North Pacific (ENP)	3.75°–16.25°N, 191.25°–268.75°E
Western North Pacific (WNP)	3.75°–16.25°N, 131.25°–178.75°E
North Indian (NI)	3.75°–21.25°N, 51.25°–108.75°E
Southern Hemisphere (SH)	18.75°–3.75°S, 61.25°–178.75°E

We do not account for interannual variability in our results [e.g., ENSO, quasi-biennial oscillation (QBO), and volcanoes], but the 34-yr period averages are expected to smooth such variability and demonstrate typical TC PI seasonal cycles in each ocean basin. To test the sampling uncertainty in the mean seasonal cycles we employ an empirical bootstrap method (e.g., Efron and Gong 1983). Bootstrapping is used to construct 1000 simulations of 34-yr subsets that are resampled from 1980 to 2013 MERRA-2 data with replacement. For each simulation we recalculate the mean seasonal cycles of SSTs and algorithm outputs (i.e., TC PI, outflow temperature, and OTL) and determine their 95% confidence intervals in each region and month. Results from this exercise show that each of these seasonal cycles averaged over the main development regions is statistically robust (see Fig. S7 and Table S1).

3. Results

a. Seasonal cycle overview

We first provide an overview of the seasonal cycles of TC PI and associated atmospheric conditions in each main development region. Figure 1 shows the seasonal cycles of sea surface temperature, outflow temperature, the outflow temperature pressure level, and TC PI for each main development region from MERRA-2 data. The seasonal cycles calculated with ERA-I data are similar to those of MERRA-2 (see Figs. S1 and S2). Figure 2 shows the horizontal structures of the monthly peak-to-peak seasonal cycle amplitudes (hereafter amplitudes) of SSTs, outflow temperature, and TC PI from MERRA-2. Positive amplitudes in Fig. 2 indicate that the seasonal cycle maximizes in the boreal summer and negative amplitudes indicate that the seasonal cycle

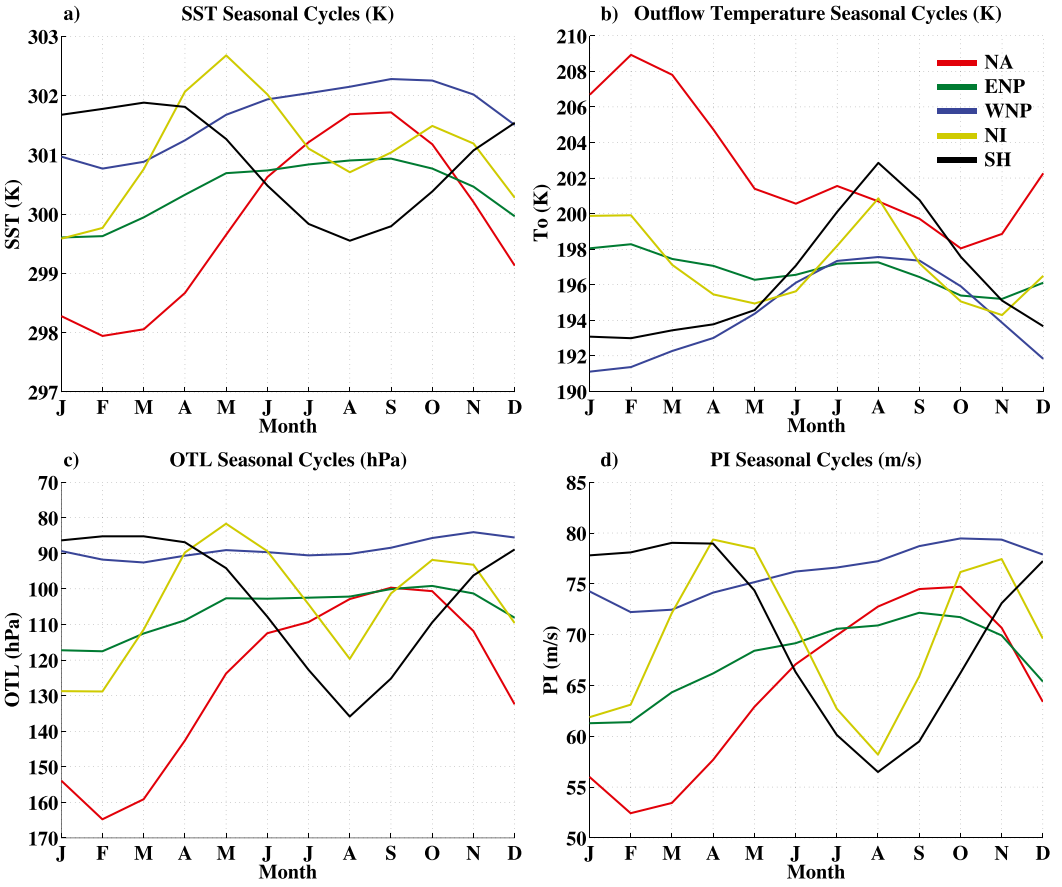

FIG. 1. Seasonal cycles of (a) SST, (b) TC outflow temperature, (c) OTL, and (d) TC PI using MERRA-2 data averaged over 1980–2013 and the TC development regions. The main development regions are NA (red), ENP (green), WNP (blue), NI (yellow), and SH (black), as defined in Table 1.

maximizes in the boreal winter; boxes outlining each main development region are also included (except NI, see below).

SST variability is driven by complex interactions in the coupled ocean–atmosphere system (e.g., Deser et al. 2010). SST seasonal cycles in the NA, ENP, WNP, and SH regions (Fig. 1a) each have a single annual maxima and a single annual minima, which coincide with their hemispheric summer or winter, respectively. The phase of the SST seasonal cycle is delayed by several months relative to the annual solar cycle owing to atmosphere–ocean thermal inertia (e.g., Cronin and Emanuel 2013). In the NI region, the monsoonal circulation drives a semiannual seasonal cycle in SSTs (Schott and McCreary 2001; Schott et al. 2009; and references therein). Because our amplitude definition does not account for a semiannual component, we do not consider the NI region in our seasonal amplitude analyses (e.g., Fig. 2; Table 2).

In the WNP, SSTs have limited seasonality (Fig. 1a) and are above the canonical 26.5°C threshold for TC development year-round (e.g., Palmén 1948; although this requisite has been recently reexamined, and its specific value is expected to increase with climate change; e.g., Vecchi and Soden 2007; Johnson and Xie 2010; McTaggart-Cowan et al. 2015). The deep mixed layer in the Pacific warm pool region results in a weak SST seasonal cycle (mean amplitude of 1.5 K) at the lower tropical latitudes (Fig. 2a; Wyrkti 1961; Schneider and Zhu 1998). The ENP region also has weak seasonality (amplitude of 1.3 K), but SSTs are cooler by 1–1.5 K (Fig. 1a) and have a less homogenous seasonal cycle across the region (Fig. 2a). The NA and SH regions both have larger seasonal amplitudes in SST (3.8 and 2.3 K, respectively) that are spatially inhomogeneous and associated with seasonally varying mixed layer depths (de Boyer Montegut et al. 2004).

Figure 3 shows the annual mean OTLs in the tropics (Fig. 3a), along with the seasonal cycles of the OTL pressure minus the lapse rate tropopause pressure averaged over each main development region (Fig. 3b). Here the lapse rate tropopause is defined as the lowest height where the lapse rate falls below 2 K km^{-1}

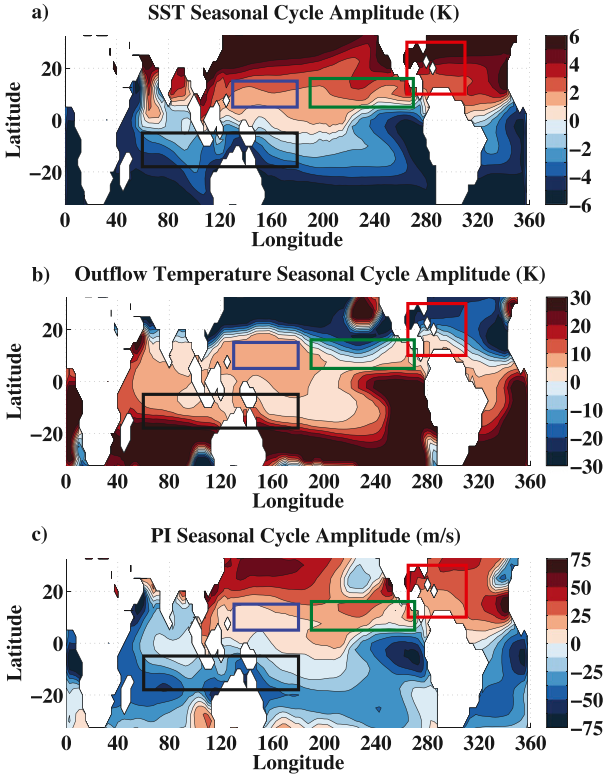

FIG. 2. Seasonal cycle monthly peak-to-peak amplitudes of (a) SSTs, (b) TC outflow temperatures, and (c) TC PI using MERRA-2 data averaged over 1980–2013. Contour intervals are every 1 K, 5 K, and 12.5 m s^{-1}, respectively. Contours saturate at each respective color bar's extent and are smoothed with a 3 × 3 gridpoint uniform boxcar filter. The main development regions indicated by boxes are WNP (blue), ENP (green), NA (red), and SH (black), as in Table 1.

(World Meteorological Organization 1957) and was determined with MERRA-2 data following the methodology of Reichler et al. (2003). A positive difference in Fig. 3b indicates that the monthly mean OTL is at a higher pressure (lower altitude) than the monthly mean tropopause. Note that the height of the tropical tropopause also has a consistent seasonal cycle: it is found at minimum pressures in the boreal winter and maximum pressures in the boreal summer (e.g., Kim and Son 2012). For reference, Fig. 4 shows the seasonal anomalies of air temperature (with the annual mean at each pressure level removed) in tropical troposphere and lower stratosphere, the lapse rate tropopause pressure, the outflow temperature levels, and the seasonal cycles of SSTs in each main development region.

The seasonal cycles in outflow temperature (Fig. 1b) are tightly linked to outflow temperature levels (Figs. 1c and 3). While the OTL remains in the troposphere, lower pressures are associated with cooler outflow temperatures (as temperatures decrease with height up to the cold point). Although there are temperature seasonal cycles in the tropical troposphere, their amplitudes on any tropospheric pressure level are small (<4 K; Fig. 4; cf. Donohoe and Battisti 2013), and instead the lapse rate and OTL pressure dominates outflow temperature seasonality. Recall that the OTL is the level of neutral buoyancy for a saturated air parcel lifted from sea level and is hence thermodynamically coupled to local SSTs (section 2; Fig. 4): warmer SSTs will be associated with higher (and therefore cooler) outflow levels, whereas cooler SSTs with be associated with lower (and warmer) outflow levels. Outflow temperatures and SSTs are therefore generally opposite phased when outflow is found in the troposphere (e.g., in the NA region from November to May; Fig. 3b). This inverse relationship has important implications for TC PI seasonality because the difference between SSTs and outflow temperatures determines the thermodynamic efficiency of the TC PI [Eq. (1)]. When the OTL migrates across the tropopause into the stratosphere, however, outflow temperatures are regulated by the lower-stratospheric temperature seasonal cycle. In each region OTLs penetrate the stratosphere at some point in the seasonal cycle, typically during their periods of largest PI (Figs. 3b–d and 4).

Annual mean OTLs in the WNP (Fig. 3a) are largely homogeneous over the region and are always found in the stratosphere (<95 hPa; Figs. 3b and 4c). This is consistent with the annual presence of the western Pacific warm pool, which "anchors" the ITCZ perennial deep convection in the west Pacific (Wytki 1961, 1989; Mitchell and Wallace 1992). In contrast, annual mean OTLs over the NA vary considerably from ~90 hPa in the southwest part of the region to ~150 hPa in the northeast. Consistent with the observed seasonal shifts of the ITCZ (Mitchell and Wallace 1992), the NA OTL only penetrates the stratosphere climatologically during the boreal summer and fall months (Figs. 3b and 4a; i.e., during the peak NA hurricane season). The other main development regions (ENP, NI, and SH) exhibit similar annual OTL inhomogeneity and seasonal variance, with their OTLs penetrating the stratosphere primarily during their peak-TC seasons (Fig. 3b). Notably, observed tropical cyclones are important and disproportionately large contributors to annual overshooting convection in the tropics, especially in the WNP (Romps and Kuang 2009). Our results suggest that TCs attaining their potential intensity would exhibit similar overshooting behavior with regionally dependent seasonal variance (Fig. 3b).

The seasonality of NA OTLs results in a large outflow temperature seasonal cycle amplitude (10.9 K) that maximizes in the boreal winter and minimizes in the boreal fall (Fig. 1b), with a considerable gradient across

TABLE 2. The monthly peak-to-peak seasonal cycle amplitudes of TC PI in each main development region (excluding NI) and the percent change in the TC PI term amplitude when either the disequilibrium or efficiency term is linearly removed [following Eq. (2)]. A negative amplitude indicates the seasonal cycle maximizes in the austral summer. A positive percentage change indicates that the term climatologically damps the TC PI seasonal cycle, whereas a negative percentage indicates that the term amplifies the TC PI seasonal cycle on average. Values are calculated using MERRA-2 data from 1980 to 2013.

Main development region	TC PI seasonal amplitude [and annual mean] ($m\,s^{-1}$)	Change when disequilibrium term is removed (%)	Change when efficiency term is removed (%)
NA	22.3 [64.6]	−72.0	−26.0
ENP	10.8 [67.6]	−84.5	−11.1
WNP	7.25 [76.1]	−58.7	26.7
SH	−22.5 [70.6]	−77.3	−21.8

the basin (Fig. 2b). The ENP and SH both have seasonal cycles of outflow temperature that are inversely related to their seasonal SSTs when their outflow is found in the troposphere, and like the NA these effects are not spatially homogenous. The semiannual cycles of NI SSTs also tracks inversely with regional average outflow temperatures when its outflow is found in the troposphere. In each region, the outflow temperature seasonal amplitude is dominated by the vertical migrations of their OTLs in the troposphere.

The perennial penetration of the WNP OTL into the stratosphere contrasts with the other regions and has important implications for WNP TC PI seasonality. By ''seeing'' the lower stratosphere year-round, WNP seasonal outflow temperatures are set by the factors controlling tropical lower-stratospheric temperatures. The seasonal cycle of tropical lower-stratospheric temperatures is annual rather than semiannual (Reed and Vlcek 1969), maximizing in the boreal summer and minimizing in the boreal winter, and is driven primarily by planetary wave forcing from the troposphere (e.g., Reid 1994; Yulaeva et al. 1994; Fueglistaler et al. 2009, 2011). Enhanced wave driving in the Northern Hemisphere compared with the Southern Hemisphere (SH) results in an annual cycle of upwelling, adiabatically cooling lower-stratospheric temperatures in the boreal winter, and warming them in the boreal summer. Recent studies have shown that this seasonal cycle is modified radiatively by the correlated upwelling of ozone, which amplifies the annual cycle by ~30% (Folkins et al. 2006; Chae and Sherwood 2007; Fueglistaler et al. 2011; Gilford and Solomon 2017). The net result is an annual cycle across the tropical lower stratosphere with an amplitude peaking at ~8 K (e.g., Reid 1994; Randel and Wu 2015). Although this seasonal cycle does not vary much in the zonal average between the two hemispheres (Fig. S5), the largest seasonal amplitudes of lower-stratospheric temperatures are found over the western Pacific and Caribbean regions, with important implications for tropical cyclones (Fig. S6; Fig. 4; see section 3b). Because the outflow of WNP TCs is always within the stratosphere (Fig. 3b), the outflow temperature seasonal cycle follows that of the lower stratosphere, maximizing in the boreal summer and minimizing in the boreal winter (Figs. 1b and 4c).

Like the WNP, the other basins show signs of lower-stratospheric influences on their monthly mean outflow temperatures in those months when their OTLs penetrate into the stratosphere (Fig. 4). Outflow

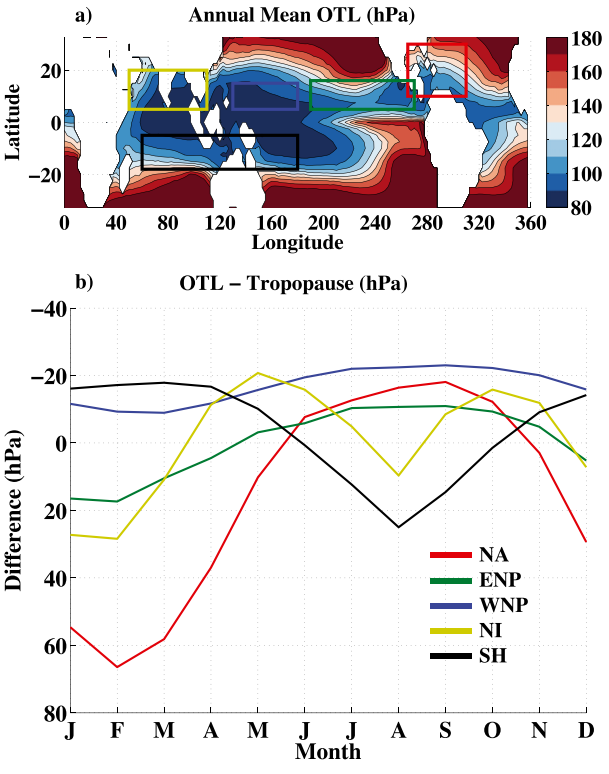

FIG. 3. (a) The annual mean OTL, computed using MERRA-2 data over 1980–2013. Contour interval is every 10 hPa. Contours saturate at the color bar's extent. (b) The seasonal cycle of the OTL minus the WMO tropopause height (hPa), using MERRA-2 data averaged over 1980–2013 and the TC main development regions defined in Table 1. Boxes and line colors follow the region convention in Figs. 1 and 2.

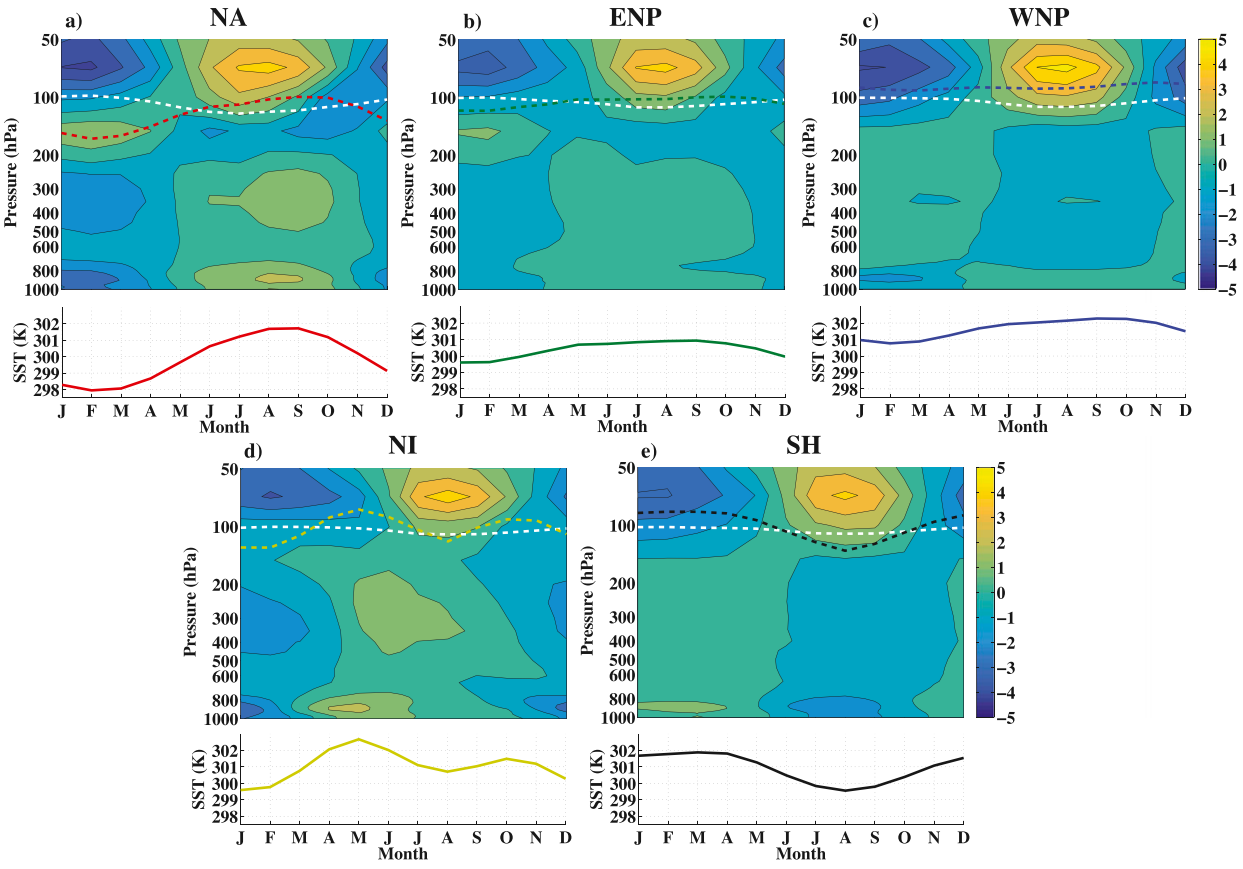

FIG. 4. (top) Seasonal anomalies of air temperature (K) at each pressure level (contours) and (bottom) seasonal cycles of sea surface temperatures (K; solid lines) for the (a) NA, (b) ENP, (c) WNP, (d) NI, and (e) SH main development regions defined in Table 1. Contour interval is every 1 K. Overlaid on the contours are seasonal cycles of the WMO lapse rate tropopause pressure (white dashed curves) and OTL (colored dashed curves). Data are from MERRA-2 averaged over 1980–2013.

temperatures in the Northern Hemisphere main development regions show similar curvature to the WNP outflow temperatures from August through November, when outflow temperatures are falling from ~198 to ~194 K following the stratospheric seasonal cycle (Figs. 1b and 4). The NA region being more poleward than the other main development regions (Table 1) results in warmer average outflow temperatures during the boreal summer and fall, delaying the NA outflow temperature minima until October (Fig. 1b). NI outflow reaches the stratosphere in both the boreal spring and fall, incidentally missing the seasonal maximum in lower-stratospheric temperatures (Fig. 4d) and resulting in an inverse relationship between SSTs and outflow temperatures in these seasons (Fig. 1b). In the months that SH OTLs are found in the stratosphere, from November through May (Figs. 3b and 4e), the magnitude and shape of the SH outflow temperatures resemble those in the WNP (Fig. 1b) and follow the lower-stratospheric seasonal cycle (Fig. 4e).

TC PI seasonality reflects regional differences in sea surface temperatures and outflow temperatures (Fig. 1d). The NA TC PI seasonal cycle has a large amplitude (~22 $m\,s^{-1}$) and maximizes in September/October, coinciding with a large amplitude seasonal cycle in SSTs. The TC PI seasonal cycles in the ENP are spatially inconsistent within the region (Fig. 2c) but on average show similar structure to their SSTs (cf. Figs. 1a,d). The SH seasonal cycle amplitude is similar to the NA (~23 $m\,s^{-1}$), maximizing in the austral fall. The NI seasonality highlights the important influence of the monsoonal circulation in setting TC potential intensity in this region. In the WNP, TC PI is strong year-round (always >72 $m\,s^{-1}$) and has a small seasonal amplitude (~6 $m\,s^{-1}$) relative to the other regions. This small amplitude indicates that either the disequilibrium term has similar weak seasonality, the thermodynamic efficiency term is damping TC PI because of stratospheric influences, or both. The relative contributions from these terms are explicitly investigated in section 3b.

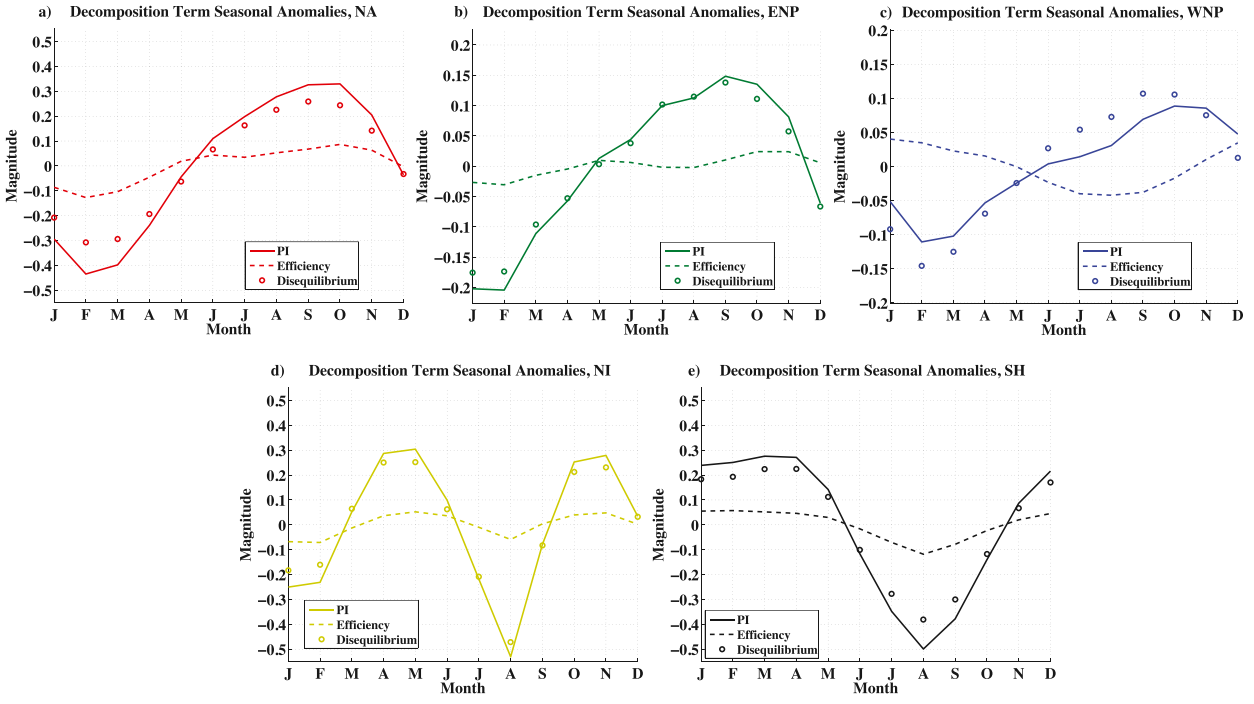

FIG. 5. Seasonal anomalies of the logarithm of TC PI times 2 [solid curves; lhs of Eq. (2)], the logarithm of thermodynamic efficiency [dashed curves; second term on rhs of Eq. (2)], and the logarithm of thermodynamic disequilibrium [circles; third term on rhs of Eq. (2)], using MERRA-2 data averaged over 1980–2013 for the (a) NA, (b) ENP, (c) WNP, (d) NI, and (e) SH TC main development regions defined in Table 1.

In contrast to the proposal of Free et al. (2004), Fig. 2c shows that TC PI seasonal cycles are not simply zonal in nature. For instance, although the ENP and WNP have similar latitudinal ranges (Table 1), they have distinct seasonal cycle structures in part because of zonal asymmetries in SSTs and outflow temperatures (Figs. 2a,b).

The TC PI seasonal cycles in Fig. 1d compare generally well with those found by Tonkin et al. (2000). In the NA, both studies find large amplitude TC PI seasonality, with values maximizing during the peak-season months (Fig. 1d). Their TC PI seasonal cycles in the low-latitude Pacific stations (equatorward of 15°N) also agree with our finding of a weak WNP TC PI seasonal cycle. Tonkin et al. (2000) also show good agreement between observed TC intensities and TC PI, and taken together our results are illustrative of why powerful TCs have been observed at all times of year in the lower latitudes of the western Pacific basin (particularly shown by Guam station data; 14°N, 145°E; their Fig. 5).

b. Potential intensity decomposition

We have shown that the seasonal cycle of WNP outflow temperatures is perennially linked to lower-stratospheric temperatures, whereas outflow temperatures in the other regions are found in the troposphere except during their peak seasons. These differences are broadly consistent with the derived TC PI in each main development region (Fig. 1d). We now employ the decomposition in Eq. (2) to specifically quantify to what extent these differences affect TC PI seasonality. Figure 5 shows the seasonal anomalies (annual means removed) of the decomposed terms averaged over the main development regions. The monthly variations in disequilibrium and efficiency terms show their specific monthly contributions to the TC PI magnitude, and these seasonal cycles are statistically robust to sampling uncertainty (Table S2). Note that $\log(C_k/C_D)$ is a constant that does not contribute to seasonal variability. Table 2 shows the TC PI seasonal cycle amplitudes (from Fig. 1d) in each region excluding the NI region, along with the percent changes in the TC PI term amplitude if the efficiency or disequilibrium term seasonal cycles are subtracted from the TC PI term seasonal cycle. A negative percent change indicates that the term climatologically amplifies the TC PI seasonal cycle, whereas a positive percent change indicates that the term climatologically damps the TC PI seasonal cycle. Percent changes do not add to 100% because of seasonal phase differences between the terms (discussed below). We see from Table 2 that in every region the disequilibrium term is the largest

overall driver of TC PI seasonality and hence always amplifies TC PI seasonal cycles.

The disequilibrium and efficiency terms in the NA (Fig. 5a) both maximize in the boreal summer/fall and minimize in the boreal winter/spring. SSTs and outflow temperatures both overall amplify the efficiency seasonality in the NA (Figs. 1a,b; Table 2), but the disequilibrium term—driven principally by SSTs—is a much larger contributor to TC PI (Table 2). Consequently, NA TC PI has strong seasonality (with an amplitude that is 35% of its annual average value) linked to the SST seasonal cycle, whereas stratospheric temperatures play a secondary role. The main influences of the NA stratospheric temperatures (when OTLs reach the stratosphere from June to October; Fig. 3b) are to slightly reduce the magnitude of the efficiency term (Fig. 5a) and slightly delay the peak month of the TC PI seasonal cycle (cf. the peak month between the NA disequilibrium term and the TC PI term). Overall the NA environment is thermodynamically most conducive for intense TCs in the boreal summer/fall, consistent with the observed NA hurricane season.

Results for the SH and ENP regions generally agree with the NA: SSTs dominate the seasonal cycle through the disequilibrium term (Figs. 5b,e), and the efficiency term is a minor amplifier (Table 2). Note that because the seasonal cycle of lower-stratospheric temperatures is similar across the tropics in both hemispheres (Fig. 4; Fig. S5), the seasonal cycle of stratospheric outflow temperatures in the SH (over November–May; Fig. 3b) amplifies the efficiency seasonal cycle (and hence TC PI) in that region rather than damping it (Table 2; Fig. 5e). TC PI in the NI region is strongly coupled to the disequilibrium term, and the efficiency term only slightly amplifies its seasonal variability (Fig. 5d).

WNP disequilibrium and efficiency terms have opposing signs and more comparable magnitudes (Fig. 5c; Table 2). The phase of the efficiency term seasonal cycle, maximizing in January–February and minimizing in August–September, is indicative that this term is principally controlled by lower-stratospheric outflow temperatures. Contributions from the disequilibrium term maximize in September–October and minimize in February, following regional SSTs (Fig. 1a). The weak seasonality of WNP SSTs (amplitude of 1.5 K) coupled with the relatively strong seasonality in lower-stratospheric outflow temperatures (amplitude of 6.4 K) allows efficiency impact to TC PI seasonality on the order of thermodynamic disequilibrium's impact (Table 2). The efficiency term damps the amplitude of the WNP TC PI seasonal cycle by about 26%. Because efficiency and TC PI are seasonally out of phase, the efficiency term's influence on PI is in fact larger than the amplitude metric shows. If, for example, the efficiency term was phase shifted by two months so that the minima in efficiency aligned with the maxima in TC PI, the WNP efficiency term would damp the TC PI seasonal cycle by 39%.

The phase offsets between the efficiency and disequilibrium terms in the WNP depress TC PI in the boreal summer. Because SSTs lagging the seasonal insolation (e.g., Braconnot et al. 2000) are offset from the asymmetric wave forcing on lower-stratospheric temperatures (e.g., Yulaeva et al. 1994), the WNP peak season occurs later than would be expected if SSTs were the only driver of WNP TC PI seasonality (shifting its TC PI maxima from September into October; Fig. 5c). The positive contribution of the NA efficiency term also delays the TC PI peak in that region, resulting in nearly equal monthly averages of NA TC PI in September and October.

To gauge the relative importance of each term in Eq. (2) between the main development regions, we examine the ratios of their amplitudes (see Table S2). If TC PI seasonality is influenced by the same factors in two regions, contributions from each term should scale consistently between those regions. Here we take the ratio of the NA and WNP term amplitudes, as they show the most dramatic contrasts in how the stratosphere impacts TC PI through the efficiency term (the NA region is characteristic of the behavior in the ENP, NI, and SH regions). We find that the amplitude ratio of NA/WNP TC PI terms is 3.8, whereas the amplitude ratios of the disequilibrium and efficiency terms are 2.2 and −2.6, respectively. Although the absolute magnitudes of their influences are different (e.g., vertical axes of Fig. 5), the differences between their proportionalities make clear that the NA seasonality (and by extension the ENP, NI, and SH regional seasonality) is strongly driven by SST seasonality through both thermodynamic disequilibrium and efficiency, whereas the WNP seasonal cycle is effectively damped by stratospheric influences on thermodynamic efficiency.

4. Summary

The seasonal cycles of tropical cyclone (TC) potential intensity (PI) have been calculated with 34 years of reanalysis data across five TC main development regions. Potential intensity depends not only on sea surface temperatures driving thermodynamic disequilibrium with the atmosphere but also on the difference between the sea surface temperatures and TC outflow temperatures (e.g., Emanuel 1985, 2003). Whereas previous studies have focused primarily on the long-term trends and interannual variability in TC PI, in this study we have elucidated the seasonality of PI and determined

the relative seasonal contributions of thermodynamic disequilibrium and thermodynamic efficiency with a decomposition method.

Environmental conditions in the western North Pacific imply that the region has perennial outflow levels that penetrate into the stratosphere and outflow temperatures that are stratospherically controlled. In contrast, outflow temperatures in the North Atlantic main development region are generally found at lower and warmer tropospheric altitudes except during the boreal summer and fall seasons (from June through October). The net result is a large-amplitude ($\sim 22\,\mathrm{m\,s^{-1}}$ from peak to peak) TC PI seasonal cycle in the North Atlantic that maximizes in the Atlantic hurricane season, compared with the weaker-amplitude but perpetually powerful ($> 70\,\mathrm{m\,s^{-1}}$) TC PI seasonal cycle in the western North Pacific. Although SSTs can be thought of as dictating the seasonal cycles in all basins, in the western North Pacific they do so in part by allowing TC outflow to be influenced by the stratosphere year-round, whereas in the other main developments regions SSTs are linked more directly to tropospheric outflow temperatures through seasonal variations in the outflow level.

Decomposing the TC PI metric reveals that thermodynamic disequilibrium is the main driver of TC PI seasonal cycles, contributing 72%–85% of the seasonal variability in each region except the western North Pacific. Thermodynamic efficiency contributions in these regions are smaller and amplify the seasonal cycle of TC PI because they are tropospherically controlled (through SSTs) during most of the year. In the western North Pacific, however, efficiency damps TC PI by between a quarter and a third because TC outflow temperatures there are linked to the seasonal cycles of lower-stratospheric temperatures, which enhance TC PI in the boreal winter and decrease it in the boreal summer. Furthermore, the stratospheric influence on western North Pacific outflow temperatures delays the peak month of TC PI by about a month relative to the peak implied by SST seasonality alone.

Our results imply that thermodynamic conditions in the western North Pacific are ripe for intense TCs throughout the year, whereas ambient conditions in the North Atlantic region typically support powerful TC intensities only during the peak hurricane season (late boreal summer and fall). In this study we have only assessed the thermodynamic conditions for intense tropical cyclones. Although powerful typhoons have been observed year-round in the western Pacific, there remains clear seasonality in their frequency (Sopko et al. 2014). This distinction is likely owing to other factors such as wind shear and midtropospheric humidity, which are not accounted for in our methodology.

Acknowledgments. The lead author thanks Allison Wing, Paul O'Gorman, Qiang Fu, and Tom Beucler for helpful discussions. We thank the anonymous reviewers whose suggestions improved this work. DG was supported by NASA Headquarters under the NASA Earth and Space Science Fellowship Program by Grant NNX14AK83H. SS, KE, and DG were supported by NSF Grant AGS-1461517.

REFERENCES

Bister, M., and K. A. Emanuel, 1998: Dissipative heating and hurricane intensity. *Meteor. Atmos. Phys.*, **65**, 233–240, doi:10.1007/BF01030791.

——, and ——, 2002: Low frequency variability of tropical cyclone potential intensity 1. Interannual to interdecadal variability. *J. Geophys. Res.*, **107**, 4801, doi:10.1029/2001JD000776.

Bosilovich, M. G., R. Lucchesi, and M. Suarez, 2016: MERRA-2: File specification. GMAO Office Note 9 (version 1.1), 73 pp. [Available online at https://gmao.gsfc.nasa.gov/pubs/docs/Bosilovich785.pdf.]

Braconnot, P., O. Marti, S. Joussaume, and Y. Leclainche, 2000: Ocean feedback in response to 6 kyr BP insolation. *J. Climate*, **13**, 1537–1553, doi:10.1175/1520-0442(2000)013<1537:OFIRTK>2.0.CO;2.

Chae, J. H., and S. C. Sherwood, 2007: Annual temperature cycle of the tropical tropopause: A simple model study. *J. Geophys. Res.*, **112**, D19111, doi:10.1029/2006JD007956.

Cronin, T. W., and K. A. Emanuel, 2013: The climate time scale in the approach to radiative–convective equilibrium. *J. Adv. Model. Earth Syst.*, **5**, 843–849, doi:10.1002/jame.20049.

de Boyer Montegut, C., G. Madec, A. S. Fischer, A. Lazar, and D. Iudicone, 2004: Mixed layer depth over the global ocean: An examination of profile data and a profile-based climatology. *J. Geophys. Res.*, **109**, C12003, doi:10.1029/2004JC002378.

Dee, D. P., and Coauthors, 2011: The ERA-Interim reanalysis: Configuration and performance of the data assimilation system. *Quart. J. Roy. Meteor. Soc.*, **137**, 553–597, doi:10.1002/qj.828.

Deser, C., M. A. Alexander, S.-P. Xie, and A. S. Phillips, 2010: Sea surface temperature variability: Patterns and mechanisms. *Annu. Rev. Mar. Sci.*, **2**, 115–143, doi:10.1146/annurev-marine-120408-151453.

Donohoe, A., and D. S. Battisti, 2013: The seasonal cycle of atmospheric heating and temperature. *J. Climate*, **26**, 4926–4980, doi:10.1175/JCLI-D-12-00713.1.

ECMWF, 2016: Interim European Centre for Medium-Range Weather Forecasts Re-Analysis (ERA-Interim). ECMWF, accessed 23 September 2016. [Available online at http://apps.ecmwf.int/datasets/.]

Efron, B., and G. Gong, 1983: A leisurely look at the bootstrap, the jackknife, and cross-validation. *Amer. Stat.*, **37**, 36–48.

Emanuel, K. A., 1985: An air–sea interaction theory for tropical cyclones. Part I: Steady-state maintenance. *J. Atmos. Sci.*, **42**, 1062–1071, doi:10.1175/1520-0469(1985)042<1062:FCITPO>2.0.CO;2.

——, 1991: The theory of hurricanes. *Annu. Rev. Fluid Mech.*, **23**, 179–196, doi:10.1146/annurev.fl.23.010191.001143.

——, 2000: A statistical analysis of tropical cyclone intensity. *Mon. Wea. Rev.*, **128**, 1139–1152, doi:10.1175/1520-0493(2000)128<1139:ASAOTC>2.0.CO;2.

——, 2003: Tropical cyclones. *Annu. Rev. Earth Planet. Sci.*, **31**, 75–104, doi:10.1146/annurev.earth.31.100901.141259.

——, 2005: Increasing destructiveness of tropical cyclones over the past 30 years. *Nature*, **436**, 686–688, doi:10.1038/nature03906.

——, 2006: Hurricanes: Tempests in a greenhouse. *Phys. Today*, **59**, 74–75, doi:10.1063/1.2349743.

——, 2007: Environmental factors affecting tropical cyclone power dissipation. *J. Climate*, **20**, 5497–5509, doi:10.1175/2007JCLI1571.1.

——, S. Solomon, D. Folini, S. Davis, and C. Cagnazzo, 2013: Influence of tropical tropopause layer cooling on Atlantic hurricane activity. *J. Climate*, **26**, 2288–2301, doi:10.1175/JCLI-D-12-00242.1.

Folkins, I., P. Bernath, C. Boone, G. Lesins, N. Livesey, A. M. Thompson, K. Walker, and J. C. Witte, 2006: Seasonal cycles of O_3, CO, and convective outflow at the tropical tropopause. *Geophys. Res. Lett.*, **33**, L16802, doi:10.1029/2006GL026602.

Frank, W. M., and E. A. Ritchie, 2001: Effects of vertical wind shear on the intensity and structure of numerically simulated hurricanes. *Mon. Wea. Rev.*, **129**, 2249–2269, doi:10.1175/1520-0493(2001)129<2249:EOVWSO>2.0.CO;2.

Free, M., M. Bister, and K. Emanuel, 2004: Potential intensity of tropical cyclones: Comparison of results from radiosonde and reanalysis data. *J. Climate*, **17**, 1722–1727, doi:10.1175/1520-0442(2004)017<1722:PIOTCC>2.0.CO;2.

Fueglistaler, S., A. E. Dessler, T. J. Dunkerton, I. Folkins, Q. Fu, and P. W. Mote, 2009: Tropical tropopause layer. *Rev. Geophys.*, **47**, RG1004, doi:10.1029/2008RG000267.

——, P. H. Haynes, and P. M. Forster, 2011: The annual cycle in lower stratospheric temperatures revisited. *Atmos. Chem. Phys.*, **11**, 3701–3711, doi:10.5194/acp-11-3701-2011.

Garner, S., 2015: The relationship between hurricane potential intensity and CAPE. *J. Atmos. Sci.*, **72**, 141–163, doi:10.1175/JAS-D-14-0008.1.

Gilford, D. M., and S. Solomon, 2017: Radiative effects of stratospheric seasonal cycles in the tropical upper troposphere and lower stratosphere. *J. Climate*, **30**, 2769–2783, doi:10.1175/JCLI-D-16-0633.1.

Gray, W. M., 1984: Atlantic seasonal hurricane frequency. Part I: El Niño and 30 mb quasi-biennial oscillation influences. *Mon. Wea. Rev.*, **112**, 1649–1668, doi:10.1175/1520-0493(1984)112<1649:ASHFPI>2.0.CO;2.

Henderson-Sellers, A., and Coauthors, 1998: Tropical cyclones and global climate change: A post-IPCC assessment. *Bull. Amer. Meteor. Soc.*, **79**, 19–38, doi:10.1175/1520-0477(1998)079<0019:TCAGCC>2.0.CO;2.

Holland, G. J., 1997: The maximum potential intensity of tropical cyclones. *J. Atmos. Sci.*, **54**, 2519–2525, doi:10.1175/1520-0469(1997)054<2519:TMPIOT>2.0.CO;2.

——, and C. L. Bruyère, 2014: Recent intense hurricane response to global climate change. *Climate Dyn.*, **42**, 617–627, doi:10.1007/s00382-013-1713-0.

Johnson, N. C., and S.-P. Xie, 2010: Changes in the sea surface temperature threshold for tropical convection. *Nat. Geosci.*, **3**, 842–845, doi:10.1038/ngeo1008.

Kim, J., and S.-W. Son, 2012: Tropical cold-point tropopause: Climatology, seasonal cycle, and intraseasonal variability derived from COSMIC GPS radio occultation measurements. *J. Climate*, **25**, 5343–5360, doi:10.1175/JCLI-D-11-00554.1.

Knutson, T. R., and Coauthors, 2010: Tropical cyclones and climate change. *Nat. Geosci.*, **3**, 157–163, doi:10.1038/ngeo779.

Kossin, J. P., 2015: Validating atmospheric reanalysis data using tropical cyclones as thermometers. *Bull. Amer. Meteor. Soc.*, **96**, 1089–1096, doi:10.1175/BAMS-D-14-00180.1.

McTaggart-Cowan, R., E. L. Davies, J. G. Fairman Jr., T. J. Galarneau Jr., and D. M. Schultz, 2015: Revisiting the 26.5°C sea surface temperature threshold for tropical cyclone development. *Bull. Amer. Meteor. Soc.*, **96**, 1929–1943, doi:10.1175/BAMS-D-13-00254.1.

Mitchell, T. P., and J. M. Wallace, 1992: The annual cycle in equatorial convection and sea surface temperature. *J. Climate*, **5**, 1140–1156, doi:10.1175/1520-0442(1992)005<1140:TACIEC>2.0.CO;2.

NASA, 2016: Modern-Era Retrospective Analysis for Research and Applications, version 2 (MERRA-2). Goddard Earth Sciences Data and Information Services Center, accessed 23 September 2016. [Available online at https://disc.sci.gsfc.nasa.gov/daac-bin/FTPSubset2.pl.]

Palmén, E., 1948: On the formation and structure of tropical hurricanes. *Geophysica*, **3**, 26–38.

Pielke, R. A., Jr., and R. A. Pielke Sr., 1997: *Hurricanes: Their Nature and Impacts on Society*. John Wiley and Sons, 279 pp.

Polvani, L. M., S. J. Camargo, and R. R. Garcia, 2016: The importance of the Montreal Protocol in mitigating the potential intensity of tropical cyclones. *J. Climate*, **29**, 2275–2289, doi:10.1175/JCLI-D-15-0232.1.

Ramsay, H. A., 2013: The effects of imposed stratospheric cooling on the maximum intensity of tropical cyclones in axisymmetric radiative–convective equilibrium. *J. Climate*, **26**, 9977–9985, doi:10.1175/JCLI-D-13-00195.1.

Randel, W. J., and F. Wu, 2015: Variability of zonal mean tropical temperatures derived from a decade of GPS radio occultation data. *J. Atmos. Sci.*, **72**, 1261–1275, doi:10.1175/JAS-D-14-0216.1.

Reichler, T., M. Dameris, and R. Sausen, 2003: Determining the tropopause height from gridded data. *Geophys. Res. Lett.*, **30**, 2042, doi:10.1029/2003GL018240.

Reed, R. J., and C. L. Vlcek, 1969: The annual temperature variation in the lower tropical stratosphere. *J. Atmos. Sci.*, **26**, 163–167, doi:10.1175/1520-0469(1969)026<0163:TATVIT>2.0.CO;2.

Reid, G. C., 1994: Seasonal and interannual temperature variations in the tropical stratosphere. *J. Geophys. Res.*, **99**, 18 923–18 932, doi:10.1029/94JD01830.

Romps, D. M., and Z. Kuang, 2009: Overshooting convection in tropical cyclones. *Geophys. Res. Lett.*, **36**, L09804, doi:10.1029/2009GL037396.

Schneider, E. K., and Z. Zhu, 1998: Sensitivity of the simulated annual cycle of sea surface temperature in the equatorial Pacific to sunlight penetration. *J. Climate*, **11**, 1932–1950, doi:10.1175/1520-0442-11.8.1932.

Schott, F. A., and J. P. McCreary Jr., 2001: The monsoon circulation of the Indian Ocean. *Prog. Oceanogr.*, **51**, 1–123, doi:10.1016/S0079-6611(01)00083-0.

——, S.-P. Xie, and J. P. McCreary, 2009: Indian Ocean circulation and climate variability. *Rev. Geophys.*, **47**, RG1002, doi:10.1029/2007RG000245.

Sobel, A. H., and S. J. Camargo, 2011: Projected future seasonal changes in tropical summer climate. *J. Climate*, **24**, 473–487, doi:10.1175/2010JCLI3748.1.

——, ——, T. M. Hall, C.-Y. Lee, M. K. Tippet, and A. A. Wing, 2016: Human influence on tropical cyclone intensity. *Science*, **353**, 242–246, doi:10.1126/science.aaf6574.

Sopko, S. P., and Coauthors, 2014: Annual tropical cyclone report. Joint Typhoon Warning Center Rep., 104 pp. [Available online

at http://www.usno.navy.mil/NOOC/nmfc-ph/RSS/jtwc/atcr/2014atcr.pdf.]

Strazzo, S. E., J. B. Elsner, and T. E. LaRow, 2015: Quantifying the sensitivity of maximum, limiting, and potential tropical cyclone intensity to SST: Observations versus the FSU/COAPS global climate model. *J. Adv. Model. Earth Syst.*, **7**, 586–599, doi:10.1002/2015MS000432.

Tonkin, H., G. J. Holland, N. Holbrook, and A. Henderson-Sellers, 2000: An evaluation of thermodynamic estimates of climatological maximum potential tropical cyclone intensity. *Mon. Wea. Rev.*, **128**, 746–762, doi:10.1175/1520-0493(2000)128<0746:AEOTEO>2.0.CO;2.

Vecchi, G. A., and B. J. Soden, 2007: Effect of remote sea surface temperature change on tropical cyclone potential intensity. *Nature*, **450**, 1066–1071, doi:10.1038/nature06423.

——, and Coauthors, 2014: On the seasonal forecasting of regional tropical cyclone activity. *J. Climate*, **27**, 7994–8016, doi:10.1175/JCLI-D-14-00158.1.

Walsh, K. J. E., and Coauthors, 2016: Tropical cyclones and climate change. *Wiley Interdiscip. Rev.: Climate Change*, **7**, 65–89, doi:10.1002/wcc.371.

Wang, S., S. J. Camargo, A. H. Sobel, and L. M. Polvani, 2014: Impact of the tropopause temperature on the intensity of tropical cyclones: An idealized study using a mesoscale model. *J. Atmos. Sci.*, **71**, 4333–4348, doi:10.1175/JAS-D-14-0029.1.

Wing, A. A., A. H. Sobel, and S. J. Camargo, 2007: Relationship between the potential and actual intensities of tropical cyclones on interannual time scales. *Geophys. Res. Lett.*, **34**, L08810, doi:10.1029/2006GL028581.

——, K. Emanuel, and S. Solomon, 2015: On the factors affecting trends and variability in tropical cyclone potential intensity. *Geophys. Res. Lett.*, **42**, 8669–8677, doi:10.1002/2015GL066145.

World Meteorological Organization, 1957: Meteorology: A three-dimensional science. *WMO Bull.*, **4**, 134–138.

Wyrtki, K., 1961: Physical oceanography of the Southeast Asian waters. Scripps Institute of Oceanography NAGA Rep. 2, 195 pp.

——, 1989: Some thoughts about the west Pacific warm pool. *Proc. West Pacific Int. Meeting and Workshop on TOGA COARE*, Noumea, Australia, Office de la Recherche Scientifique et Technique Outre-Mer, 99–109.

Yulaeva, E., J. R. Holton, and J. M. Wallace, 1994: On the cause of the annual cycle in tropical lower-stratospheric temperatures. *J. Atmos. Sci.*, **51**, 169–174, doi:10.1175/1520-0469(1994)051<0169:OTCOTA>2.0.CO;2.